INTERNATIONAL JOURNAL FOR NUMERICAL METHODS IN FLUIDS
Int. J. Numer. Meth. Fluids 2001; **37**: 375–397 (DOI: 10.1002/fld.74)

A finite volume–multigrid method for flow simulation on stratified porous media on curvilinear co-ordinate systems

Pablo Calvo*,[1] and Francisco Lisbona[2]

Depto. de Matemática Aplicada, Universidad de Zaragoza, C/Pedro Cerbuna 12, Zaragoza, Spain

SUMMARY

This paper presents a numerical study of infiltration processes on stratified porous media. The study is carried out to examine the performance of a finite volume method on problems with discontinuous solutions due to the transmission conditions in the interfaces. To discretize the problem, a curvilinear co-ordinate system is used. This permits matching the interface with the boundary of the control volumes that interchange fluxes between layers. The use of the multigrid algorithm for the resulting systems of equations allows problems involving a large number of nodes with low computational cost to be solved. Finally, some numerical experiments, which show the capillary barrier behaviour depending on the material used for the different layers and the geometric design of the interface, are presented. Copyright © 2001 John Wiley & Sons, Ltd.

KEY WORDS: capillary barrier; curvilinear mesh; finite volume method

1. INTRODUCTION

With the sharp increase in industrial activity, the production of harmful materials for disposal has increased. These materials, along with the massive utilization of agricultural fertilizers, are polluting underground waters. The design and simulation of natural devices that inhibit the flows that transport surface water pollution to the phreatic stratum have enormous environmental significance. One such device is based on the superposition of material layers with very different hydraulic properties. Flow retention at the interface is created by the capillary barrier effect. When the interface presents a slope, the infiltrated flow from the upper surface is laterally diverted due to the retention in the normal to the interface direction; consequently, this flow can be drained. Several sloping stratified layers make a natural protection mechanism against infiltration.

* Correspondence to: Depto. de Matemática Aplicada, Edificio de Matematicas, 1 planta, C./Pedro Cerbuna 12, Universidad de Zaragoza, 50009 Zaragoza, Spain.
[1] E-mail: pablo@andres.unizar.es
[2] E-mail: lisbona@posta.unizar.es

Received July 1998
Revised January 1999

This paper focuses on the flow into stratified unsaturated soils and attempts to provide an appropriate numerical method to simulate the retention effect that may take place near the surface between layers. We simulate the flux due to diffusive and gravity effects on a domain composed of two regions with different properties, separated by a curve (surface) with a parametric representation. A finite volume technique is used for the discretization of the equations and the resulting non-linear systems are solved by applying multigrid schemes.

A numerical approximation for the one-dimensional unsaturated flow in stratified media into very dry soils has been performed in Reference [1] using a water content formulation. Oldenburg *et al.* [2] have examined the ability of different finite difference techniques using the pressure formulation of the problem with the quasi-linear approach to represent flow exclusion and leakage effects at capillary barriers.

An interface equation treatment is proposed in such a way that mass conservation is preserved. This interface treatment is combined with a curvilinear co-ordinate system, which allows us to fit the grids to the imposed geometry on the boundaries and the interface.

The rest of the paper deals with the following aspects. We construct a numerical model using a finite volume discretization of the problem, paying special attention to the transmission conditions. To do this, a regular transformation maps the physical domain onto a square computational domain, where the numerical discretization is carried out. The interface requires a precise treatment of the finite volume integration at each level and of the definition of the restriction and prolongation operators. These operators relate the discrete solutions between different grids (levels). Finally, using the van Genuchten model, some numerical experiments are performed showing non-saturated flow behaviour under the interface presence.

2. GOVERNING EQUATIONS

A two-dimensional model, made up of two homogeneous consolidated media occupying disjoint bounded open sets Ω_1 and Ω_2 with piecewise regular boundaries, is considered. Ω_1 and Ω_2 are separated by a surface defined by a common boundary Γ.

The macroscopic scale movement is formulated by the mass conservation equation and the momentum equation. The mass conservation equation can be expressed as $(\rho^k\theta^k)_{,t} + (\rho^k q_j^k)_{,j} = 0$, where the comma denotes differentiation, t is the time, x_j are the Cartesian co-ordinates, θ^k is the volumetric content of the phase k ($k = \mathrm{w}$ for water, $k = \mathrm{a}$ for air), ρ^k is the specific mass of the phase k, and q_j^k is the velocity of that phase in the Darcy sense, i.e. the discharge per unit bulk cross-section. The formulation is simplified due to the following assumptions: (i) the water is incompressible and the air pressure is taken constant as $p_\mathrm{a} = 0$, so capillary pressure $p_\mathrm{c} = p_\mathrm{a} - p_\mathrm{w} = -p_\mathrm{w}$; (ii) the flow is isothermal, so the thermal effects of viscous dissipation are neglected and no water phase changes are considered; (iii) the water flow is slow enough for the validity of Darcy's generalized law; and (iv) no sink and source terms are considered.

Darcy's equation relates the flux and the pressure gradients by

$$\mathbf{q} = -\mathbf{K}(\theta)\nabla(-\psi + z) \tag{1}$$

where $\psi = -p_w/(g\rho_w)$ is the capillary pressure head, $\mathbf{q}$ is the water flux, and $\mathbf{K}(\theta)$ is the diagonal tensor that represents the hydraulic conductivity. Hereafter, we will consider hydraulic properties as tensors, and only in the test cases will homogeneous and isotropic soil assumption be applied.

Introducing Darcy's law into the continuity equation and supposing a unique non-linear relation $\psi = \psi(\theta)$ (known as the retention curve) leads to the Richards equation for each medium

$$\frac{\partial \theta}{\partial t} = \nabla(\mathbf{D}^1(\theta)\nabla\theta + \mathbf{K}^1(\theta)\nabla z) \quad \text{in } \Omega_1 \tag{2}$$

$$\frac{\partial \theta}{\partial t} = \nabla(\mathbf{D}^2(\theta)\nabla\theta + \mathbf{K}^2(\theta)\nabla z) \quad \text{in } \Omega_2 \tag{3}$$

The transmission conditions are the capillary pressure continuity

$$\psi^1(\theta^+) = \psi^2(\theta^-) \quad \text{on } \Gamma \tag{4}$$

and the flux continuity

$$(\mathbf{D}^1(\theta)\nabla\theta + \mathbf{K}^1(\theta)\nabla z)\cdot\mathbf{n} = (\mathbf{D}^2(\theta)\nabla\theta + \mathbf{K}^2(\theta)\nabla z)\cdot\mathbf{n} \quad \text{on } \Gamma \tag{5}$$

Here $\mathbf{D}^i(\theta) = \text{diag}(D^i_x(\theta), D^i_z(\theta)) = -\mathbf{K}^i(\theta)(\partial\psi^i/\partial\theta)$ is the capillary diffusivity tensor in Ω_i, $\mathbf{n}$ is the Ω_2 outer normal vector to Γ, and θ^+ and θ^- are the θ values on Γ taken from the domains Ω_1 and Ω_2 respectively. Let us note that the pressure continuity condition involves a discontinuity in the transmission condition for the saturation variable. The initial condition is for $t = 0$ and the boundary conditions complete the problem.

This problem can be also dealt with a formulation based on the water pressure variable p_w. The use of a pressure formulation is natural because no discontinuities appear in the interfaces; however, in coarse-grained dry soils, some disadvantages are reported for this formulation in References [1,3]. Because of this, a water content formulation is chosen. Moreover, this formulation has better mass conservation properties [4].

The geometry of the problem is depicted in Figure 1. To apply the finite volume technique, the use of a curvilinear co-ordinate system will allow us to work on a simpler computational domain. Let $\mathbf{r}^i_l(\eta)$, $\mathbf{r}^i_r(\eta)$, $\mathbf{r}^i_t(\xi)$, $\mathbf{r}^i_b(\xi)$: $[0, 1] \to \mathbf{R}^2$, $i = 1, 2$ be four parametric curves per domain that match $\partial\Omega_i$ (Figure 1). Corner angles in the global domain are assumed not to be far from orthogonality. Otherwise, due to the mesh generation strategy, almost degenerated finite volumes can appear giving convergence problems. In our computations, if finite volumes with angles less than 50° are present in the discretization, convergence behaviour deteriorates. At this point, a theoretical study is required to estimate the influence of the deformation of the grid on the convergence.

These parametric equations are interpreted as the transformations that map the unitary square boundaries onto the physical domain boundaries. Let us assume that derivatives satisfy $(\mathbf{r}^i_l)'$, $(\mathbf{r}^i_r)'$, $(\mathbf{r}^i_t)'$, $(\mathbf{r}^i_b)' \neq 0$ and $\mathbf{r}^2_t(\xi) = \mathbf{r}^1_b(\xi) = \Gamma$ (l ≡ left, r ≡ right, t ≡ top and b ≡ bottom).

Let Φ^i: $\Delta = [0, 1] \times [0, 1] \to \Omega_i$, $i = 1, 2$ be twice-differentiable regular transformations, given by [8]

$$\begin{aligned}(x(\xi, \eta), z(\xi, \eta)) = \Phi^i(\xi, \eta) = (1-\eta)\mathbf{r}_{\mathrm{b}}^i(\xi) + \eta\mathbf{r}_{\mathrm{t}}^i(\xi) + (1-\xi)\mathbf{r}_{\mathrm{l}}^i(\eta) + \xi\mathbf{r}_{\mathrm{r}}^i(\eta) \\ - (\xi\eta\mathbf{r}_{\mathrm{t}}^i(1) + \xi(1-\eta)\mathbf{r}_{\mathrm{b}}^i(1) - \eta(1-\xi)\mathbf{r}_{\mathrm{t}}^i(0) \\ - (1-\xi)(1-\eta)\mathbf{r}_{\mathrm{b}}^i(0))\end{aligned} \tag{6}$$

The Δ domain will be taken as the computational or reference domain, where we will consider a rectangular mesh.

The hosted equations can be obtained by transforming the Richards equations to the reference domain. The Jacobian of Φ^i is

$$J_{\Phi^i} = J = x_\xi z_\eta - x_\eta z_\xi \neq 0 \tag{7}$$

For a function $g(x, y) = g(x(\xi, \eta), y(\xi, \eta)) = \tilde{g}(\xi, \eta)$, the transformation of the derivatives can be written as

$$g_x = \frac{\tilde{g}_\xi z_\eta - \tilde{g}_\eta z_\xi}{J}, \qquad g_z = \frac{\tilde{g}_\eta z_\xi - \tilde{g}_\xi z_\eta}{J} \tag{8}$$

or in a conservative form as

$$\begin{aligned} g_x &= \frac{1}{J}\left((\tilde{g}z_\eta)_\xi - (\tilde{g}z_\xi)_\eta\right) \\ g_z &= \frac{1}{J}\left((\tilde{g}x_\xi)_\eta - (\tilde{g}x_\eta)_\xi\right) \end{aligned} \tag{9}$$

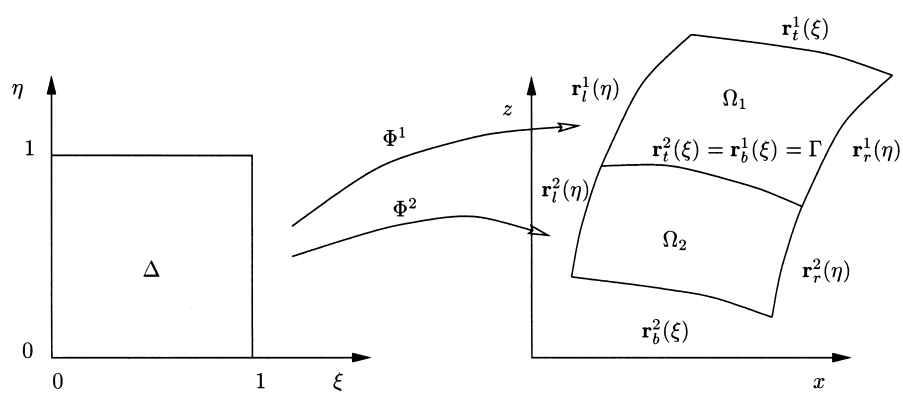

Figure 1. Physical domain transformations.

Using Equation (8) to transform θ_x, we have

$$D_x\theta_x = \frac{\tilde{D}_x}{J}(\tilde{\theta}_\xi z_\eta - \tilde{\theta}_\eta z_\xi) \tag{10}$$

and using Equation (9) to transform

$$\left(\frac{\tilde{D}_x}{J}(\tilde{\theta}_\xi z_\eta - \tilde{\theta}_\eta z_\xi)\right)_x \tag{11}$$

we obtain a conservative expression for the x-direction diffusive term expressed in the new variables

$$J(D_x\theta_x)_x = \left(\frac{\tilde{D}_x}{J}(\tilde{\theta}_\xi z_\eta - \tilde{\theta}_\eta z_\xi)z_\eta\right)_\xi - \left(\frac{\tilde{D}_x}{J}(\tilde{\theta}_\xi z_\eta - \tilde{\theta}_\eta z_\xi)z_\xi\right)_\eta \tag{12}$$

and the same for the z-direction. Convection terms are transformed in a similar way. If the original equations are multiplied by the Jacobian and then transformed to $\xi\eta$ co-ordinates using the derived formulas, the resulting equations are

$$J^i\frac{\partial\theta}{\partial t} = (\alpha^i\theta_\xi)_\xi + (\beta^i\theta_\xi)_\eta + (\beta^i\theta_\eta)_\xi + (\gamma^i\theta_\eta)_\eta + (K_z^i(\theta)x_\xi)_\eta - (K_z^i(\theta)x_\eta)_\xi \tag{13}$$

with the coefficients given by

$$\alpha^i = \frac{D_x^i(\theta)z_\eta^2 + D_z^i(\theta)x_\eta^2}{J^i}, \qquad \beta^i = -\frac{D_x^i(\theta)z_\xi z_\eta + D_z^i(\theta)x_\xi x_\eta}{J^i}$$

$$\gamma^i = \frac{D_x^i(\theta)z_\xi^2 + D_z^i(\theta)x_\xi^2}{J^i} \tag{14}$$

where i is the parameter that labels the medium Ω_1 or Ω_2 and the tilde ($\sim$) notation is dropped.

3. FINITE VOLUME DISCRETIZATION OF GOVERNING EQUATIONS

Let us define a grid $\Delta^h = (\xi_i, \eta_j)$ on Δ at a given level by the non-uniform partitions

$$\xi_0 = 0 < \xi_1 < \cdots < \xi_N = 1 \quad \text{and} \quad \eta_0 = 0 < \eta_1 < \cdots < \eta_M = 1$$

The control volumes are defined by the lines that connect the mid-points between nodes. Its co-ordinates are (Figure 2)

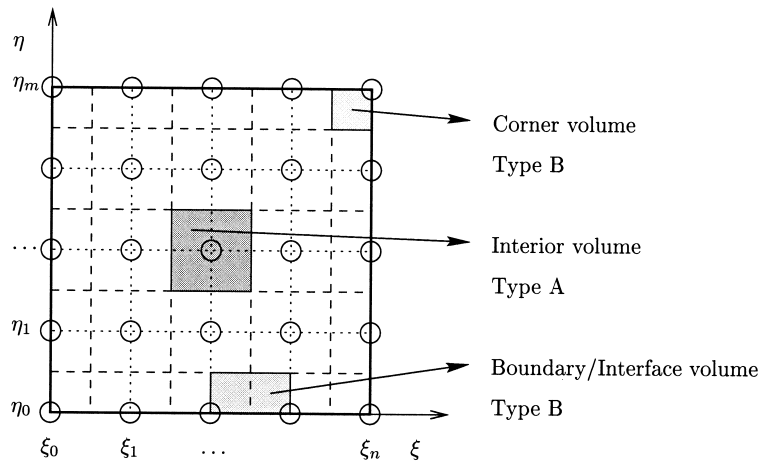

Figure 2. Discretization of the computational domain.

$$\xi_{i+1/2} = \xi_i + \frac{1}{2}\delta\xi_i, \qquad \delta\xi_i = \xi_{i+1} - \xi_i, \quad i = 0, \ldots, N-1$$

$$\eta_{j+1/2} = \eta_j + \frac{1}{2}\delta\eta_j, \qquad \delta\eta_j = \eta_{j+1} - \eta_j, \quad j = 0, \ldots, M-1 \tag{15}$$

In Ω there are interior, boundary and corner volumes. Interior volumes have the nodes in the mid-point, boundary volumes (including the interface volumes) have the node over the boundary and corner volumes locate the node just in the corner.

For an interior control volume centred at ξ_i and η_j, the $\Delta\xi_i = \xi_{i+1/2} - \xi_{i-1/2}$ and $\Delta\eta_j = \eta_{j+1/2} - \eta_{j-1/2}$ dimensions are defined, where $\xi_{-1/2} = \xi_0$, $\xi_{N+1/2} = \xi_N$ and $\eta_{-1/2} = \eta_0$, $\eta_{M+1/2} = \eta_M$. The time span $[0, T]$ is discretized by the non-uniform grid $0 = t_0 < t_1 < \cdots < t_L = T$. For simplicity, P will be a generic point whose co-ordinates are (ξ_i, η_j) and θ_{P}^k represents the water content at P and in the time t_k. Likewise, the nodes that are located at the east, west, north and south will be denoted as E, W, N and S, and the nodes located at $\xi_{i\pm1/2}$, $\eta_{j\pm1/2}$ co-ordinates (at the finite volume faces) will be denoted using the lower-case letters e, w, n and s, as in Figure 3. The variables related to such points will be written using the corresponding subscript. For example, $\alpha_e = \alpha|_{(\xi,\eta)=(\xi_{i+1/2},\eta_j)}$.

The differential equation is integrated at every finite volume $V \equiv [\xi_{i-1/2}, \xi_{i+1/2}] \times [\eta_{j-1/2}, \eta_{j+1/2}]$ (Reference [9])

$$\iint_V J\frac{\partial\theta}{\partial t} = \iint_V (\nabla_{\xi\eta}\cdot(\Lambda\nabla_{\xi\eta}\theta) + (K(\theta)x_\xi)_\eta - (K(\theta)x_\eta)_\xi) \tag{16}$$

where

$$\Lambda = \begin{pmatrix} \alpha & \beta \\ \beta & \gamma \end{pmatrix}$$

The time discretization of Equation (16) can be done by using the following scheme:

$$\frac{J_{\mathrm{P}}\Delta\xi_i\Delta\eta_j}{\tau_k}(\theta_{\mathrm{P}}^{k+1} - \theta_{\mathrm{P}}^{k}) = r_1F_1(t_{k+1}) + (1-r_1)F_1(t_k) + r_2F_2(t_{k+1}) + (1-r_2)F_2(t_k) \tag{17}$$

where $\tau_k = t^{k+1} - t^k$; $r_i \in [0, 1]$, $i = 1, 2$; $F_1 = \iint_V \nabla_{\xi\eta} \cdot (\Lambda \nabla_{\xi\eta}\theta)$; and $F_2 = \iint_V [(K(\theta)x_\xi)_\eta - (K(\theta)x_\eta)_\xi]$.

Approximating space derivatives with incremental quotients, where the corner values on the finite volume are computed using a bilinear interpolation of the grid values

$$\theta_{ne} = \frac{\theta_{\mathrm{P}} + \theta_{\mathrm{E}} + \theta_{\mathrm{N}} + \theta_{\mathrm{NE}}}{4}$$

$$\theta_{nw} = \frac{\theta_{\mathrm{P}} + \theta_{\mathrm{W}} + \theta_{\mathrm{N}} + \theta_{\mathrm{NW}}}{4}$$

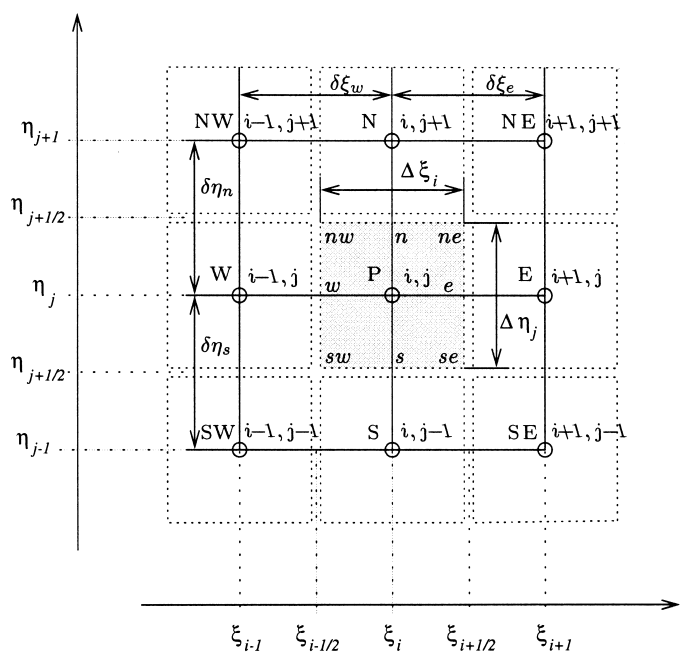

Figure 3. Finite volume.

$$\theta_{se} = \frac{\theta_{\mathrm{P}} + \theta_{\mathrm{E}} + \theta_{\mathrm{S}} + \theta_{\mathrm{SE}}}{4}$$

$$\theta_{sw} = \frac{\theta_{\mathrm{P}} + \theta_{\mathrm{W}} + \theta_{\mathrm{S}} + \theta_{\mathrm{SW}}}{4}$$

the integration of the differential equation over the finite volume results in the following totally discrete scheme:

$$\frac{J_{\mathrm{P}}}{\tau_k}\Delta\xi\Delta\eta\theta_{\mathrm{P}}^{k+1} - r_1\sum_{i\in\mathscr{S}} c_i\theta_i^{k+1} - r_2 d(\theta^{k+1}) = \frac{J_{\mathrm{P}}}{\tau_k}\Delta\xi\Delta\eta\theta_{\mathrm{P}}^{k} + (1-r_1)\sum_{i\in\mathscr{S}} c_i\theta_i^{k} + (1-r_2)d(\theta^{k}) \tag{18}$$

with $\mathscr{S} = \{\mathrm{P}, \mathrm{E}, \mathrm{W}, \mathrm{N}, \mathrm{S}\}$ as the set of points of the spatial stencil. The coefficients c_i are

$$c_{\mathrm{P}} = -\frac{\alpha_e\Delta\eta}{\delta\xi_e} - \frac{\alpha_w\Delta\eta}{\delta\xi_w} - \frac{\gamma_n\Delta\xi}{\delta\eta_n} - \frac{\gamma_s\Delta\xi}{\delta\eta_s}$$

$$c_{\mathrm{E}} = \frac{\alpha_e\Delta\eta}{\delta\xi_e} + \frac{\beta_n - \beta_s}{2}$$

$$c_{\mathrm{W}} = \frac{\alpha_w\Delta\eta}{\delta\xi_w} - \frac{\beta_n - \beta_s}{2}$$

$$c_{\mathrm{N}} = \frac{\gamma_n\Delta\xi}{\delta\eta_n} + \frac{\beta_e - \beta_w}{2}$$

$$c_{\mathrm{S}} = \frac{\gamma_s\Delta\xi}{\delta\eta_s} - \frac{\beta_e - \beta_w}{2}$$

$$d(\theta) = (K_z(\theta_n)x_{\xi n} - K_z(\theta_s)x_{\xi s})\Delta\xi - (K_z(\theta_e)x_{\eta e} - K_z(\theta_w)x_{\xi w})\Delta\eta \tag{19}$$

For the boundary volumes located at the right side we take, $e = \mathrm{P}$, $ne = n$, $se = s$, modifying the discretization accordingly. Similar conditions can be applied for the remaining three boundaries of the domain. The discretization at the corners are handled in a similar way, where now the variables located over the two boundary walls are shifted.

4. INTERFACE EQUATIONS

The finite volume method formulates a numerical approximation to the differential equation by constructing flux balances across faces limiting the control volumes. At the interior finite volumes, the numeric evaluation of the outlet flux across a face involves variables located at both sides. When the adjacent volume is integrated, the same flux (inlet) is evaluated using the

same variables (and coefficients) so flux continuity is ensured. The strategy used in this work for the interface treatment is based on the flux continuity preservation across it.

Let us denote $\mathbf{n} = (n_x, n_z)$ the outer normal vector to Ω_2 on the interface Γ. The normal flux crossing the interface is

$$-D_x\left(\frac{\partial\theta}{\partial x}\right)n_x - D_z\left(\frac{\partial\theta}{\partial z}\right)n_z - K_z n_z = \frac{\theta_\xi}{J}\left(-D_x n_x z_\eta + D_z n_z x_\eta\right) + \frac{\theta_\eta}{J}\left(D_x n_x z_\xi - D_z n_z x_\xi\right) - K_z n_z$$
$$= \beta\theta_\xi + \gamma\theta_\eta + K_z x_\xi \tag{20}$$

where dependencies are not explicitly written to simplify the notation.

Let us consider Δ when it is the reference domain of Ω_2, and a reference control volume with its north face laying on $\eta = 1$. In this case, the volume integration over the divergence of the flux terms in the Richards equation is carried out by substituting the flux expression at the interface face by its value computed using only data corresponding to the Ω_1 domain. The discrete equation for these volumes is very similar to Equation (18) but the quantities associated with the flux crossing the interface have been collected in a special term f

$$k_t\theta_{\mathrm{P}}^{k+1} - r_1\left(\sum_{i\in\mathscr{S}} c_i\theta_i^{k+1} + f^{k+1}\right) - r_2 d(\theta^{k+1})$$
$$= k_t\theta_{\mathrm{P}}^{k} + (1-r_1)\left(\sum_{i\in\mathscr{S}} c_i\theta_i^{k} + f^{k}\right) + (1-r_2)d(\theta^k) \tag{21}$$

where the stencil $\mathscr{S} = \{\mathrm{P}, \mathrm{E}, \mathrm{W}, \mathrm{S}\}$ does not include the node N, $k_t = J_{\mathrm{P}}\Delta\xi\,\Delta\eta/\tau_k$, and the coefficients c_i are

$$c_{\mathrm{P}} = -\frac{\alpha_e\Delta\eta}{\delta\xi_e} - \frac{\alpha_w\Delta\eta}{\delta\xi_w} - \frac{\gamma_s\Delta\xi}{\delta\eta_s} + \frac{\beta_e - \beta_w}{2}$$

$$c_{\mathrm{E}} = \frac{\alpha_e\Delta\eta}{\delta\xi_e} + \frac{-\beta_s}{2}$$

$$c_{\mathrm{W}} = \frac{\alpha_w\Delta\eta}{\delta\xi_w} - \frac{-\beta_s}{2}$$

$$c_{\mathrm{S}} = \frac{\gamma_s\Delta\xi}{\delta\eta_s} - \frac{\beta_e - \beta_w}{2}$$

$$d(\theta) = -K_z(\theta_s)x_{\xi s}\Delta\xi - \left(K_z(\theta_e)x_{\eta e} - K_z(\theta_w)x_{\xi w}\right)\Delta\eta \tag{22}$$

The term f is the approximation of the flux $\beta\theta_\xi + \gamma\theta_\eta + K_z x_\xi$ evaluated in Δ as the Ω_1 reference domain. When the reference volume is taken at the other side (in Ω_1), the discretization is treated in a similar way on the line $\eta = 0$ over the south faces.

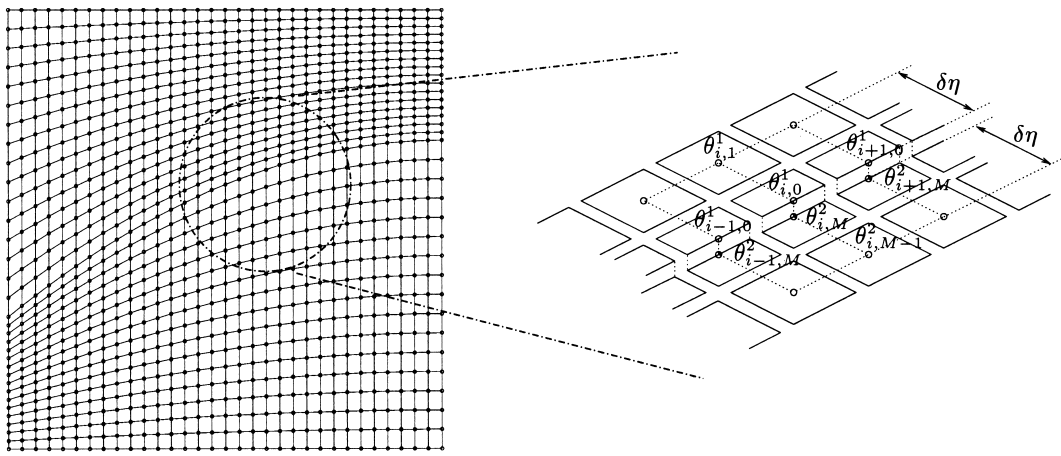

Figure 4. Interface treatment.

From now on, two different volumes will be distinguished, the so-called type A volumes, where none of their boundaries and the interface match up, and the type B volumes, where some of their boundaries and the interface coincide (Figures 2 and 4). Let us take a type B volume located above the interface as the sample volume. Therefore, the flow through the *east* face is expressed to be proportional to the incremental quotient $(\theta_{\mathrm{E}} - \theta_{\mathrm{P}})/\delta\xi_e$ where $\theta_{\mathrm{P}} = \theta^1_{i,0}$ (the superscript will indicate the domain) and $\theta_{\mathrm{E}} = \theta^1_{i+1,0}$ are in the same domain, where the properties are continuous throughout the $\xi = cte$ interface line. The same procedure is valid for the *west* face. For the *south* face, in contrast, to preserve mass conservation for the calculation of the flow crossing that face, θ_η is computed as $(\theta^2_{i,M} - \theta^2_{i,M-1})/\delta\eta^*_s$, i.e. both variables are located in the domain Δ as the Ω_2 reference domain ($\delta\eta^*_s = \eta_M - \eta_{M-1}$). Note that θ_η is not computed as $(\theta^1_{i,0} - \theta^2_{i,M})/\delta\eta_s$ because $\theta^1_{i,0}$ is at $(\xi^1_i, \eta^1_0) \in \Delta_1$, $\theta^2_{i,M}$ is at $(\xi^2_i, \eta^2_{j^*}) \in \Delta_2$ and $\delta\eta_s = 0$ for all ξ_i.

If boundary conditions impose a flux, at the face of the boundary volumes we can use the discrete expressions derived for the interface, setting f to the value of the imposed flux. For Dirichlet boundary conditions, the nodes over the boundary have a known value and no equation is required.

The *explicit* time integration scheme results from $r_1 = r_2 = 0$. This is the simpler method because the time marching scheme only requires function evaluations. Explicit schemes suffer from a severe stability constraint (Courant–Friedrichs–Lewy (CFL) restrictions). The time step has to be chosen very small in order to restrict excessive error growth. Totally *implicit* methods are obtained when r_1 and r_2 are both not zero. As they are unconditionally stable, the time increment is only limited by accuracy requirements. The A-stable method of order two, which supplies the smallest error constant, is the trapezoidal rule, also known as the Crank–Nicholson method. The system of Equations (18) and (19) can be linearized and be solved using a linear system solver, such as Gauss–Seidel or conjugate gradient (CG) for

non-symmetric matrices based algorithms [11]. A particular and interesting simplification is obtained when all coefficients are evaluated in the last iteration and r_2 is taken equal to 0. The derived method is classified as a *semi-implicit* method. Because only convection terms are treated explicitly, they provide a CFL condition that is weaker than the corresponding one to the totally explicit scheme. In this paper, we have chosen the implicit scheme for the resolution of the problem, possibly involving a large number of unknowns, due to its good convergence properties. The complexity of this problem is handled with an efficient solver, such as a multigrid method.

5. MULTIGRID METHOD

Multigrid methods differ from classic iterative methods because multigrid schemes make use of a set of nested grids. The final approximation to the solution is obtained on the finer grid and this grid is the same as that used by one-grid methods. Multigrid method efficiency lies on the interaction between the *smoothing* on the fine grid and the *coarse grid correction*. Some error components are reduced on the fine grid and some others are reduced on the coarse grids [10].

Let us define a nested grid sequence $\Omega^{h_0} \subset \Omega^{h_1} \subset \cdots \subset \Omega^{h_l}$ where Ω^{h_l} is the finer grid. The h-subscript is called the *level number*. The coarsest grid consists of a reduced amount of points. The $\Omega^{h_{i+1}}$ grid is defined by halving the step size of the Ω^{h_i} grid.

Multigrid schemes for non-linear problems are well known; therefore, only special features of this interface problem will be described.

The non-linear problem at every level l can be formally expressed as $\mathscr{L}^{h_l}(\theta^{h_l}) = f^{h_l}$, where $\mathscr{L}^{h_l}$ is a non-linear operator $\mathscr{L}^{h_l}$: $\mathbf{G}(\Delta_1^{h_l}) \cup \mathbf{G}(\Delta_2^{h_l}) \to \mathbf{G}(\Delta_1^{h_l}) \cup \mathbf{G}(\Delta_2^{h_l})$, and $\mathbf{G}(\Delta_i^{h_l})$ is the space of grid functions on $\Delta_i^{h_l}$. The dimension of $\mathbf{G}(\Delta_i^{h_l})$ is $(N_l+1)(M_l+1)$. Consequently, there are $(N_l+1)(M_l+1)$ discrete θ^{h_l} values. f^{h_l} is the right-hand side of the equation to be solved that collects the explicit term in the discretization values plus the boundary conditions. The multigrid methods proceeds as follows:

nlmgm($\hat{\theta}$, θ, f, l)

```
begin
if l = l_0 then
   S•_{l_0}(θ̂_{l_0}, θ_{l_0}, f_{l_0}, l_0)
else
   /*pre-smoothing*/
   S^{ν1}_l(θ̂_l, θ_l, f_l, l)
   /*compute defect*/
   d_l := f_l − L_l θ_l
   choose: θ̂_{l−1}, s_{l−1}
   /*defect restriction*/
   f_{l−1} := L_{l−1}(θ̂_{l−1}) − s_{l−1} I_l^{l−1} d_l
   for κ := 1 to γ* do
      nlmgm(θ̂_{l−1}, θ_{l−1}, f_{l−1}, l − 1);
```



```
    if (κ < γ*) then θ̂_{l-1} ← θ_{l-1}
  /*prolongation and correction*/
    θ_l := θ_l + (1/s_{l-1}) I^l_{l-1}(θ_{l-1} − θ̂_{l-1})
  /*post-smoothing*/
  S^{ν2}_l(θ̂_l, θ_l, f_l, l)
end
```

$\mathscr{S}_l^{\nu}$ means the smoothing procedure that performs ν iterations at level l over Δ^{h_l}. On the numerical test, the smoothing procedure consists of a Gauss–Seidel iteration over the entire domain including the described interface treatment. The resolution of the non-linear problem at that lowest level iterating to convergence is denoted as $\mathscr{S}_{l_0}^{\bullet}$. Level 0 corresponds to the coarsest grid and therefore to the smallest system of equations. As a result, it can be solved using the iterative method employed in the smoothing process due to the fast convergence for small number of unknowns. $\hat{\theta}$ and θ are the proposed and the computed approximation respectively in the *nlmgm* iteration. f is the right-hand side term and $I_l^{l_j}$ is the operator that transfers the solution from Δ^{h_i} to Δ^{h_j}. If Δ^{h_i} is finer than Δ^{h_j}, then the operator is called *restriction*, and if Δ^{h_i} is coarser than Δ^{h_j}, the operator is called *interpolation* or *prolongation*. The variable γ^* is the number of coarse corrections at the level $l-1$, and s is a damping parameter ($s \approx 0.7$) used only in the first iterations to improve convergence.

5.1. Smoothing operator

At each level l we have a system of equations like Equations (18) and (19) and (21) and (22), with $2(N_l+1)(M_l+1)$ unknowns and one equation per unknown (note that N_l+1 grid points over the interface give $2N_l+2$ unknowns, N_l+1 at each domain). This system can be written as

$$A(\boldsymbol{\theta}^{k+1})\boldsymbol{\theta}^{k+1} = B(\boldsymbol{\theta}^k)\boldsymbol{\theta}^k + \mathbf{c} \tag{23}$$

where $\boldsymbol{\theta}^{k+1}$ is the unknowns vector with the lexicographic order $\theta_0 = \theta^{k+1}_{\{0,0\}}, \theta_1 = \theta^{k+1}_{\{0,1\}}, \ldots, \theta_n = \theta^{k+1}_{\{0,n\}}, \theta_{n+1} = \theta^{k+1}_{\{1,0\}}, \ldots, A = A(\boldsymbol{\theta}^{k+1})$ is a matrix that can be decomposed as

$$A = \begin{pmatrix} A_{11} & A_{12} \\ A_{21} & A_{22} \end{pmatrix}, \quad A_{11}, A_{22} \in \mathbf{R}^{(N_l+1)\times(M_l+1)} \tag{24}$$

and $B(\boldsymbol{\theta}^k)\boldsymbol{\theta}^k + \mathbf{c}$ is the right-hand side vector collecting the source terms, the terms evaluated at time t_k and the boundary conditions. The matrix $B(\boldsymbol{\theta}^k)$ has the same structure as $A(\boldsymbol{\theta}^{k+1})$. The sparse A matrix has the structure depicted in Figure 5 and the sub-matrices A_{12}, A_{21} collect the terms related to the interface normal flux computation.

The smoothing process is carried out using a classic iterative method. For this purpose, every equation is linearized: non-linear terms are evaluated with values that have been updated on the last iteration. A Gauss–Seidel scheme is applied as the iterative method where every unknown is updated using the corresponding equation. If the unknown corresponds to one of

the interface nodes, the value of the unknown corresponding to the same node and located in the other domain is modified using the retention curve in order to impose the pressure correction. The complete updating process is described through the following algorithm:

Gauss–Seidel

```
begin
/*Domain Δ1*/
for i := Ml down to 1 do
   for j := 0 to Nl do
      S^1_{i,j}
/*Interface treatment*/
for sweeps := 1 to maxSweeps do
   for j := 0 to Nl do
      S^1_{0,j};
      θ^2_{Ml,j} ← (ψ^2)^{-1}(ψ^1(θ^1_{0,j}))
   for j := 0 to Nl do
      S^2_{Ml,j};
      θ^1_{0,j} ← (ψ^1)^{-1}(ψ^2(θ^2_{Ml,j}))
/*Domain Δ2*/
for i := Ml − 1 down to 0 do
   for j := 0 to Nl do
      S^2_{i,j}
end
```

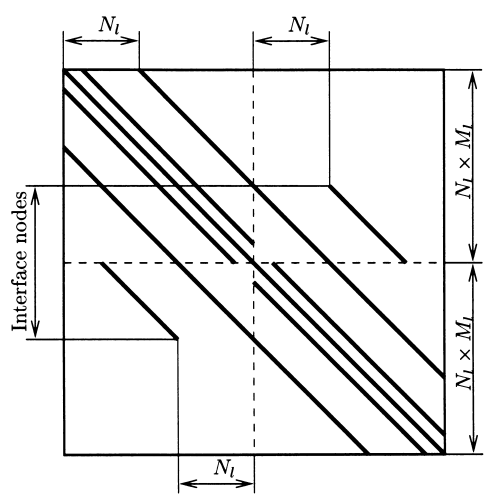

Figure 5. Structure of the coefficient matrix.

Here $\mathscr{S}^s_{i,j}$ denotes the application of the discrete equation for the correction of the $\theta^s_{i,j}$ value ($s = 1, 2$ denoting variables in Ω_1 and Ω_2); ψ relates the water content to the capillary pressure; and *maxSweeps* is the maximum number of interface iterations.

Multigrid methods occasionally apply local smoothing techniques. These ones are necessary when a small set of variables deteriorates the global convergence (e.g. sharp gradients occurrence or corners in the geometry). In our case, some extra iterations over the interface variables can be performed.

5.2. Prolongation and restriction

The restriction operator I_l^{l-1} and the prolongation operator I_{l-1}^l map grid functions between two grids. Figure 6 represents two grids $\Delta^{h_{l-1}}$ and Δ^{h_l}. All grids are nested and match the interface at every level. The highest level grid (the fine grid) is represented by the symbol $+$. The next level (the coarse grid) is represented by $\times$. The control volumes on the fine grid are plotted using a dotted line ($\cdots$) and the volumes on the coarse grid are plotted using a dashed line ($- - -$). Because $\Delta^{h_{l-1}} \subset \Delta^{h_l}$, the coarse grid nodes are drawn over the fine grid points (Δ is Δ_1 or Δ_2).

The restriction operator is taken by the trivial injection

$$\begin{aligned} I_l^{l-1} &: \mathbf{G}(\Delta^{h_l}) \to \mathbf{G}(\Delta^{h_{l-1}}) \\ &: \boldsymbol{\theta}^{h_l}(x) \rightsquigarrow \boldsymbol{\theta}^{h_{l-1}}(\mathbf{x}) = \boldsymbol{\theta}^{h_l}(\mathbf{x}) \end{aligned}$$

for all $\mathbf{x} \in \Delta^{h_{l-1}} \subset \Delta^{h_l}$. The trivial injection has been used because it preserves the mass at the boundary volumes better than more complex projection operators. The prolongation operator is taken as a piecewise bilinear interpolation. Let us first consider the situation of Figure 6 and

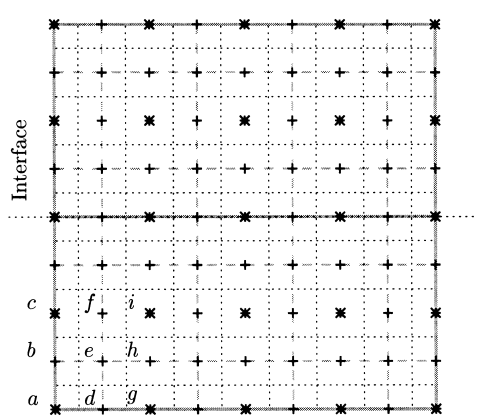

Figure 6. Two-level discretization.

assume $\xi \in [0, 1]$, where $j = a, b, \ldots, h, i$ are the co-ordinates of the points depicted in the figure. $\mathbf{x}_j \in \Delta^{h_l - 1} \cap \Delta^{h_l}$ for $j = a, c, g, i$ are the coarse grid nodes. At the coarse grid points the values remain unchanged:

$$\boldsymbol{\theta}^{h_l}(\mathbf{x})_j = \boldsymbol{\theta}^{h_l - 1}(\mathbf{x})_j, \quad j = a, c, g, i$$

For the points b, d, f and h lying directly between coarse grid points, linear interpolation results in

$$\boldsymbol{\theta}^{h_l}(\mathbf{x})_b = \frac{1}{2}\boldsymbol{\theta}^{h_l - 1}(\mathbf{x})_a + \frac{1}{2}\boldsymbol{\theta}^{h_l - 1}(\mathbf{x})_c$$

$$\boldsymbol{\theta}^{h_l}(\mathbf{x})_d = \frac{1}{2}\boldsymbol{\theta}^{h_l - 1}(\mathbf{x})_a + \frac{1}{2}\boldsymbol{\theta}^{h_l - 1}(\mathbf{x})_g$$

$$\theta^{h_l}(\mathbf{x})_f = \frac{1}{2}\boldsymbol{\theta}^{h_l - 1}(\mathbf{x})_c + \frac{1}{2}\boldsymbol{\theta}^{h_l - 1}(\mathbf{x})_i$$

$$\boldsymbol{\theta}^{h_l}(\mathbf{x})_h = \frac{1}{2}\boldsymbol{\theta}^{h_l - 1}(\mathbf{x})_g + \frac{1}{2}\boldsymbol{\theta}^{h_l - 1}(\mathbf{x})_i$$

It remains to define $\boldsymbol{\theta}^{h_l}$ at the centre $\mathbf{x}_e$ as

$$\mathbf{x}_e = \frac{1}{4}(\boldsymbol{\theta}^{h_l - 1}(\mathbf{x})_a + \boldsymbol{\theta}^{h_l - 1}(\mathbf{x})_c + \boldsymbol{\theta}^{h_l - 1}(\mathbf{x})_g + \boldsymbol{\theta}^{h_l - 1}(\mathbf{x})_i)$$

6. COMPUTATIONAL RESULTS AND DISCUSSION

The techniques described in the previous section have been checked on a variety of tests problems for a stratified soil composed of two layers represented by Ω_1 and Ω_2. The first layer Ω_1 consists of a fine sand and Ω_2 of a loamy clay. The obtained results will be taken into account for the construction of a more realistic problem, where an infiltration protection system is designed.

Curvilinear co-ordinate systems make possible the use of the scheme on a wide variety of geometries. Some horizontal straight interfaces and sloping (straight and curvilinear) interfaces will be simulated. Experiment 1 shows the retention effect and it has been used to check that the influence of the interface on the time step is almost negligible. Experiments 2, 3 and 4 (Table II) having a sloping interface showing the power and the flexibility of the co-ordinate transformation for checking the diverting behaviour of the interface.

The correlation model used for the water retention curves and the hydraulic conductivity is the proposed by van Genuchten [5].

$$S = \frac{\theta - \theta_r}{\theta_s - \theta_r} = \left(\frac{1}{1 + (\alpha\psi)^n} \right)^m$$

$$K(\theta) = K_s \theta^{1/2} (1 - (1 - \theta^{1/m})^m)^2 \tag{25}$$

where θ_r and θ_s are the residual and the saturation of the soil respectively; α, n, m are characteristic parameters that have to be adjusted with empirical results; and K_s is the hydraulic conductivity under saturation conditions. The constants used for the simulations are shown in Table I and m is computed as $m = 1 - (1/n)$.

The geometry of the test problems is depicted in Figure 7. $\Omega_1 \cup \Omega_2$ is a rectangle of $x_r \times z_t$ dimensions divided by Γ. The Γ curve has the start point at $(0, z_l)$, the end point at (x_r, z_r) and is chosen in $\mathscr{P}_2$ (polynomials of degree ≤ 2)

$$\Gamma(\xi) = (\xi x_r, z_r + (z_r - z_l)\xi + 4k(\xi - \xi^2)) \tag{26}$$

where $\xi \in [0, 1]$. This curve is taken to be an increasing (or decreasing) function, and then k is bounded by $|k| \leq |(z_r - z_l)/4|$. The co-ordinates z_l and z_r are set to the values shown in Table II.

Table I. van Genuchten correlation constants.

Material	θ_r	θ_s	α (cm^{-1})	n	K_s (cm day^{-1})
Clay (Ω_1)	0.1060	0.4686	0.0104	1.3954	13.1
Sand (Ω_2)	0.0286	0.3658	0.0280	2.2390	541.0

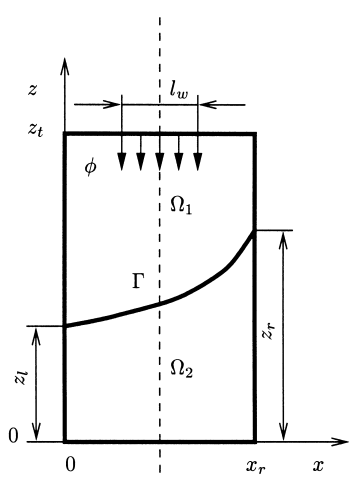

Figure 7. Geometry of the numerical tests 1–4.

Table II. Γ curve parameters.

Case	z_l	z_r	k	z_t	x_r	l_w
1	250	250	0	500	500	250
2	150	350	0	500	500	500
3	150	350	50	500	500	500
4	150	350	−50	500	500	500

At the l level of the multigrid method, each grid $\Delta_i^{h_l}$, $i = 1, 2$ has the same number of nodes $(2^{l+1}+1)(2^l+1)$. Then, the global domain has $2(2^{l+1}+1)(2^l+1)$ nodes, where $(2^{l+1}+1)$ nodes are overlapped on the interface. If a one-grid solver, such the Gauss–Seidel, is applied, then only the finer grid is used. $l = 4$ is the highest level used in the different case test problems. The implemented multigrid algorithm uses the meshes corresponding to levels $l = 4, 3, 2, 1$. In order to reduce the computational cost, metric coefficients, Jacobians, areas and mesh widths are pre-computed and stored for further use through the simulation.

In Table III, we present some indicators to show the advantage of the multigrid scheme over the use of the one-level solver. We also include the results of two computations with five and six levels (in a shorter time simulation) to highlight that the ratio multilevel cost/one-level cost is higher for finer grids.

Initial conditions are specified setting the capillary pressure head as constant over the global domain. Because of the presence of the discontinuity of the hydraulic properties, the domain composed by sand is drier than the clay domain. To avoid the van Genuchten correlations degenerating, the saturation in the clay medium is set to 0.1. Therefore, the saturation of the sand medium is computed using the retention curves that result two orders of magnitude smaller.

A flux of 0.1 cm day^{-1} is injected through a window of size l_w centred on the top of the domain Ω_1. This flux is maintained constant during the simulation. In all cases, the time step is initially chosen as $\tau_0 = 0.8$ days and r_1, r_2 parameters are chosen as 0.5.

The simulation implements a time step strategy. If the iterative method needs more than ten iterations, the time step is reduced by the factor 0.9 and if it takes less than three iterations then the method is allowed to increase the time step by the factor 1.05. The time reduction occurs when the waterfront reaches the interface or high water content gradients are present.

Table III. Computational resources.

l	Method	Time per integration (s)	Iterations per step	Time per step (s)	Memory per field	Nodes per field
4	Gauss–Seidel	1.6	9	13	220 kb	4290
4	Multigrid	2.7	3	8.1	481 kb	5838
5	Gauss–Seidel	5.1	15	77	840 kb	16 770
5	Multigrid	8.6	3	25	1.3 Mb	22 608
6	Gauss–Seidel	20.5	27	553	3.3 Mb	66 306
6	Multigrid	34.8	4	140	4.5 Mb	88 914

Comparing this method and that of Hills [1,6], the present method improves the numerical efficiency of the interface treatment. The two-dimensional version of the Reference [1] scheme shows an important time step reduction when the water reaches the interface [7].

6.1. Geometry influence on diversion capacity

Figure 8 shows the approximate solutions at $t = 712$ and 822 days, where the length units are metres. In this case, l_w is half of the top boundary length; therefore, two-dimensional effects can be observed. The β mesh parameter is zero in $\bar{\Omega}_1 \cup \bar{\Omega}_2$ so no grid distortion is present. In this case, the left panel shows how the water content has reached the interface (at $z = z_l = z_r = 250$ cm) and contour lines are orthogonal to the interface because the retention effect. At $t = 822$ days (right panel), the water has been accumulated in the centre of the domain over the interface. Some amount of water passes through and the vertical flux is in accordance with the presence of non-orthogonal contour lines (0.32 line).

Three additional simulations have been performed with sloping interface. The curve is chosen as in Equation (26). The extreme values $k = \pm (z_b - z_a)/4$ correspond to the case where a maximum or a minimum is found at the boundary, i.e. $\Gamma'(0) = 0$ or $\Gamma'(1) = 0$. These extreme values have been chosen at simulations 3 and 4. Therefore, simulations 2, 3 and 4 take $k = 0$, $k = 50$ (maximum value) and $k = -50$ cm (minimum value) respectively. The three simulations include as a top boundary condition, the flow infiltration along the whole top boundary with a 0.1 cm day^{-1} inlet flux.

In the case $k = 0$ cm, $\Gamma(\xi)$ is straight and the angle is $\arctan(2/5) \approx 21.8°$. Figures 9–11 show how most of the flow is diverted to the left side and how some infiltration occurs near the right boundary. Close to the interface, the direction of the saturation gradient is modified and it becomes almost parallel to the discontinuity. Comparing cases 2 and 3, case 3 exhibits a larger amount of water intrusion in the Ω_2 domain. This is due to the waterfront reaching the interface region with a reduced slope. Furthermore, the convexity of the interface results in a reduced Ω_1 volume and a lower storage capacity.

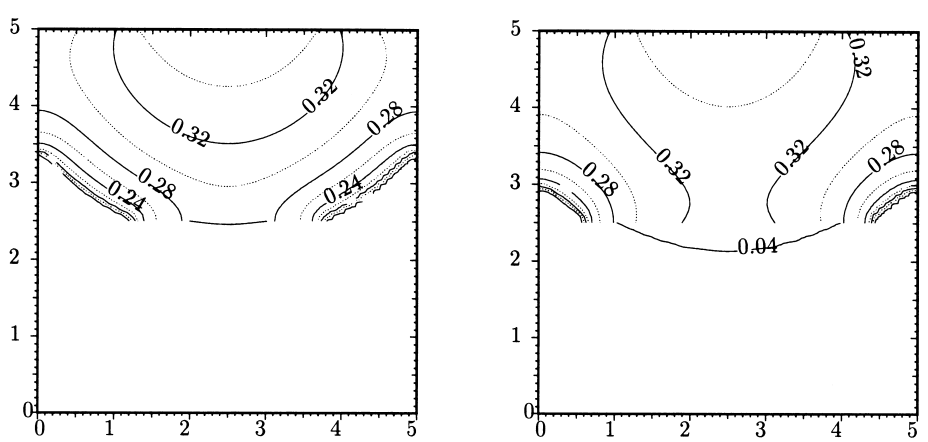

Figure 8. Case 1.

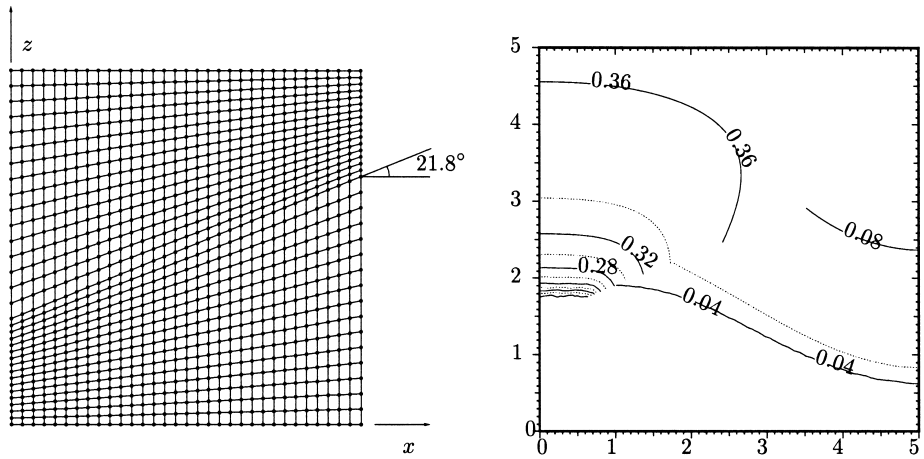

Figure 9. Case 2; $k = 0$ cm.

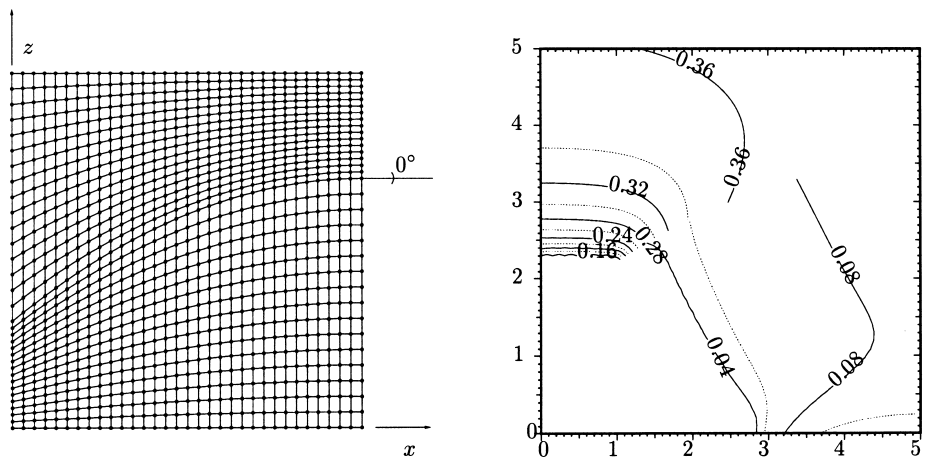

Figure 10. Case 3; $k = 50$ cm.

The last simulation corresponds to case 4 (Figure 11). This is even more effective than the straight interface. The right end at Γ is the first interface point that the waterfront reaches. The slope at this point is $\Gamma'(1)$ that for $k = -50$ cm corresponds approximately to an angle of 38.7°. This angle is larger than for the straight interface and avoids water accumulation at the top of the interface. For $t = 712$ days, case 4 presents a better diversion capacity than case 2. Even if the slope at the left hand is not as sharp as the straight interface, the flow direction is already oriented and makes this barrier system more effective.

6.2. Material properties influence on diversion capacity

Capillary barrier effects take place when very different hydraulic properties are present in the interface. An infiltration protection system based on the capillary barrier phenomena needs to take into account not only a high rate between the hydraulic properties but also an appropriate conductivity selection of the upper materials to allow water to move laterally. This second criteria can be checked with the following two experiments. A gravel with a very high hydraulic conductivity ($K_s = 30240$ cm day^{-1}) is covered with two sands, the first one has a lower conductivity ($K_s = 171$ cm day^{-1}) than the second one ($K_s = 320$ cm day^{-1}). In the first case, the conductivity rate is higher than in the second one, so a higher retention effect is expected; however, as we will see, it is not the best choice for a barrier system. Figure 12 shows the simulations for two configurations. The first one makes use of sand 1 for Ω_1 and gravel for Ω_2. The second simulation is obtained by substituting sand 1 with sand 2 (Table IV). In both cases, the straight interface starts at (0, 200) and it has an angle of 5°. The first configuration (left panel) hardly allows the water flow to the left boundary. The second one (right panel), because of the higher hydraulic conductivity, shows that the water is accumulated at the left side with no water intrusion into Ω_2.

6.3. A protection system configuration

In this section we check the chosen materials with different geometries in a more realistic problem. The geometry and the computational grid is depicted on the left sides of Figures 13–15, while saturation (not water content) is shown in the right panels. The three configurations correspond to one straight interface and two curved interfaces. The height increment for a width of 500 cm of the layer must be small. This means that the diversion capacity has to be good enough to push water laterally. This increment is 61.4 cm that corresponds to 7°.

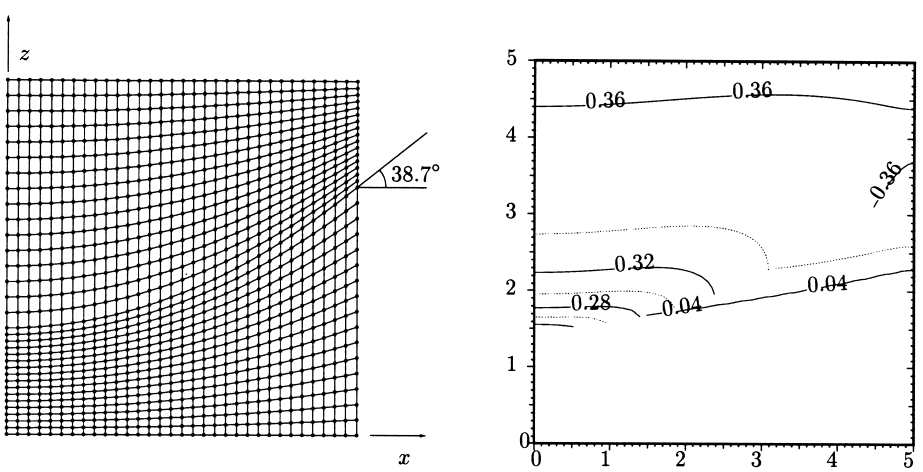

Figure 11. Case 4; $k = -50$ cm.

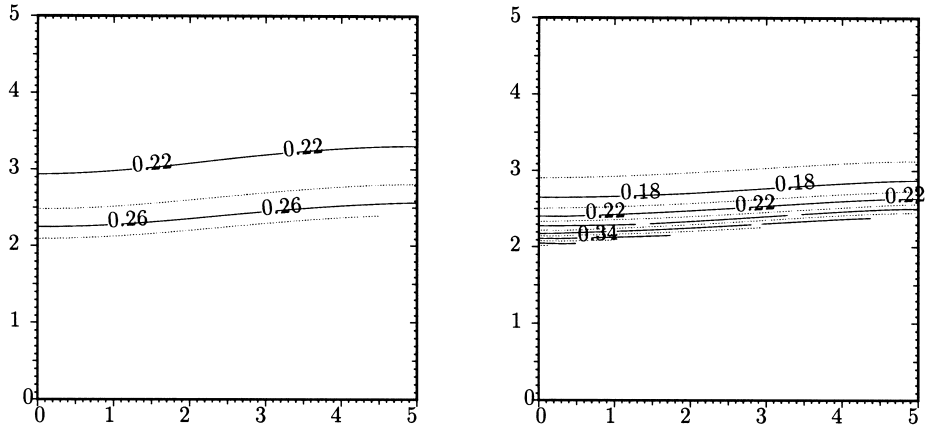

Figure 12. Case 5.

Table IV. van Genuchten correlation constants for Case 5.

Material	θ_r	θ_s	α (cm^{-1})	n	K_s (cm day^{-1})
Sand 1	0.0834	0.3248	0.0411	1.3826	171.5
Sand 2	0.0300	0.4500	0.0494	1.7900	320.0
Gravel	0.0050	0.4190	4.9300	2.1900	30240.0

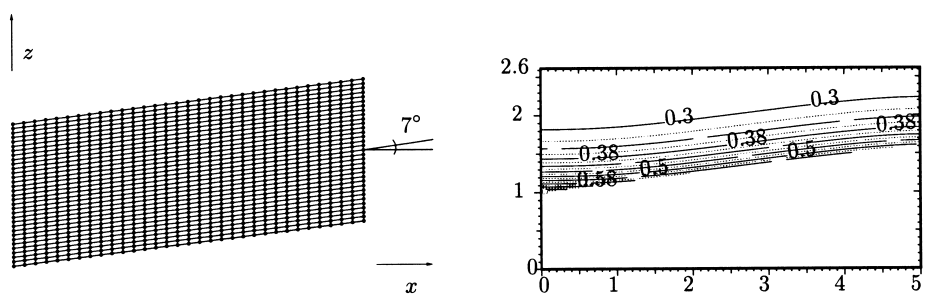

Figure 13. Case 6.

Three simulations have been done over this configuration with the gravel at Ω_2 and the sand 2 (chosen at the previous experiment) at Ω_1. The results show that the best configuration is the last one (case 8). Water reaches the interface and is diverted laterally due to the presence of the slope. In the last experiment, the slope is more important where the material is more saturated; this happens at the left side. These results are not suggested by the solution of case 3. The

reason for this apparent discrepancy is due to the dominance of the gravity effects over the boundary injection when hydraulic conductivity is higher. This effect can be observed in the water content gradient. In this experiment, water content infiltrates faster and the saturation is higher close to the interface rather than at the top boundary. The k parameter is chosen as ± 7.67404, which ensures that approximately half of the angle $\arctan(61.4/500) = 7°$ is at (x_r, z_r). The straight interface is an inter-medium situation, which shows as an advantage a simpler construction.

7. CONCLUSIONS

According to a possible non-Cartesian geometry of the domain and the interface, the Richards equation has been formulated into a curvilinear co-ordinate system. Each sub-domain, consisting of a homogeneous material is mapped onto a square domain through a regular transformation. For the discretization, a vertex-centred finite volume technique has been used. The interface treatment considers the pressure continuity and the normal flow continuity. This flow is evaluated entirely at the adjacent domain.

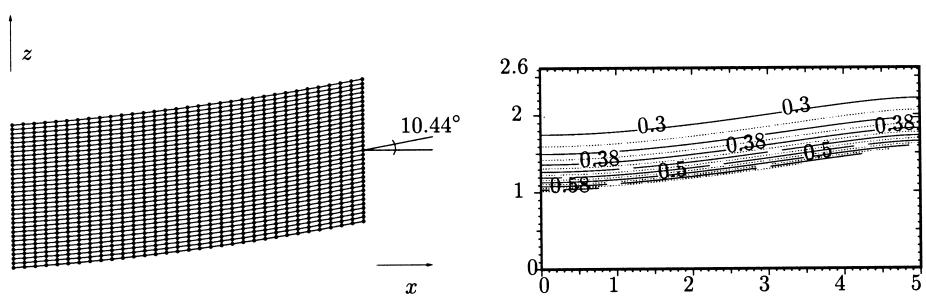

Figure 14. Case 7.

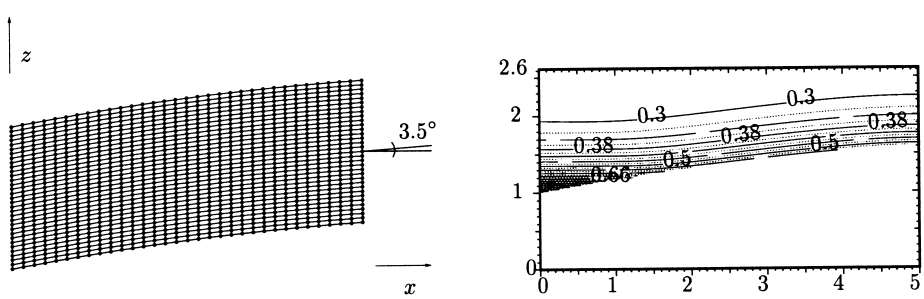

Figure 15. Case 8.

Several situations have been considered. For the first one, the interface is horizontal and the inlet flow is injected through a window and it allows the retention effect due to the interface presence to be checked. The rest of the simulations compare the flow for different domains, interface shapes, and hydraulic properties.

The numerical scheme provides a time–space approximation that preserves the water mass conservation. The obtained numerical approximation represents the expected solution of the saturation variable at the discontinuity, and it requires a relatively low computational cost because of the multigrid efficiency and the local smoothing possibility at the discontinuity to improve global convergence. The numerical treatment adopted over the transmission condition at the interface does not generate time step limitations under very low saturation conditions in one of the domains. (These limitations have been observed using a cell-centred discretization.)

Because of the nature of the interface treatment it is possible to implement the method using parallel techniques for non-overlapping domain decomposition.

REFERENCES

1. Hills RG, Porro I. Modeling one-dimensional infiltration into very dry soils 1. Model development and evaluation. *Water Resources Research* 1989; **25**(6): 1259–1269.
2. Oldenburg CM, Pruess K. On numerical modeling of capillary barriers. *Water Resources Research* 1993; **29**(4): 1045–1056.
3. Huyakorn PS, Pinder GF. *Computational Methods in Subsurface Flow*. Academic Press: San Diego, CA, 1983.
4. Rathfelder K, Abriola LM. Mass conservative numerical solutions of the head-based Richards equation. *Water Resources Research* 1996; **30**(9): 2579–2586.
5. van Genuchten MTh. A closed-form equation for predicting the hydraulic conductivity of unsaturated soils. *Soil Science Society of America Journal* 1980; **44**: 892–898.
6. Hills RG, Porro I. Modeling one-dimensional infiltration into very dry soils 2. Estimation of the soil water parameters and model predictions. *Water Resources Research* 1989; **25**(6): 1271–1282.
7. Calvo P, Lisbona F, Pétriz F. Simulación numérica de flujos no saturados en medios estratificados mediante un método de volúmenes finitos. In *Actas 3er Congreso de Métodos Numéricos en Ingeniería*, 1996; 1625–1636.
8. Knupp P, Steinberg S. *Fundamentals of Grid Generation*. CRC Press: Boca Raton, FL, 1994.
9. Patankar SV. *Numerical Heat Transfer and Fluid Flow*. Hemisphere: New York, 1980.
10. Hackbusch W. *Multi-grid Methods and Application*, *Springer Series in Computational Mathematics*, vol. 4. Springer: Berlin, 1985.
11. Sorin A, Ruel F. Assessment of some iterative methods for non-symmetric linear systems arising in computational fluid dynamics. *International Journal for Numerical Methods in Fluids* 1995; **21**(12): 1171–1200.

